

Temperature-Dependent Kinetics Studies of the Reactions $\text{Br}(^2\text{P}_{3/2}) + \text{CH}_3\text{SCH}_3 \leftrightarrow \text{CH}_3\text{SCH}_2 + \text{HBr}$. Heat of Formation of the CH_3SCH_2 Radical

A. Jefferson,^{†‡} J. M. Nicovich,[†] and P. H. Wine^{*,†,§,⊥}

Georgia Tech Research Institute, School of Chemistry and Biochemistry, and School of Earth and Atmospheric Sciences, Georgia Institute of Technology, Atlanta, Georgia 30332

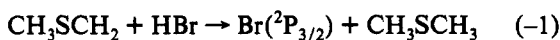
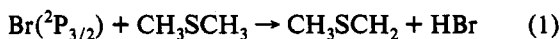
Received: November 2, 1993[⊙]

Time-resolved resonance fluorescence detection of $\text{Br}(^2\text{P}_{3/2})$ atom disappearance or appearance following 266-nm laser flash photolysis of $\text{CF}_2\text{Br}_2/\text{CH}_3\text{SCH}_3/\text{H}_2/\text{N}_2$ and $\text{Cl}_2\text{CO}/\text{CH}_3\text{SCH}_3/\text{HBr}/\text{H}_2/\text{N}_2$ mixtures has been employed to study the kinetics of the reactions $\text{Br}(^2\text{P}_{3/2}) + \text{CH}_3\text{SCH}_3 \leftrightarrow \text{HBr} + \text{CH}_3\text{SCH}_2$ (1, -1) as a function of temperature over the range 386–604 K. Arrhenius expressions in units of $\text{cm}^3 \text{ molecule}^{-1} \text{ s}^{-1}$ which describe the results are $k_1 = (9.0 \pm 2.9) \times 10^{-11} \{\exp[(-2386 \pm 151)/T]\}$ and $k_{-1} = (8.6 \pm 2.5) \times 10^{-13} \{\exp[(836 \pm 140)/T]\}$; errors are 2σ and represent precision only. To our knowledge, these are the first kinetic data reported for each of the two reactions studied. Second and third law analyses of the equilibrium data for reactions 1 and -1 have been employed to obtain the following enthalpies of reaction in units of kcal mol^{-1} : $\Delta H_{298} = 6.11 \pm 1.37$ and $\Delta H_0 = 5.37 \pm 1.38$. Combining the above enthalpies of reaction with the well-known heats of formation of Br, HBr, and CH_3SCH_3 gives the following heats of formation of the CH_3SCH_2 radical in units of kcal mol^{-1} : $\Delta H_{f,298} = 32.7 \pm 1.4$ and $\Delta H_{f,0} = 35.3 \pm 1.4$; errors are 2σ and represent estimates of absolute accuracy. The C–H bond dissociation energy in CH_3SCH_3 obtained from our data, $93.7 \pm 1.4 \text{ kcal mol}^{-1}$ at 298 K and $92.0 \pm 1.4 \text{ kcal mol}^{-1}$ at 0 K, agrees well with a recent molecular beam photofragmentation study but is 3 kcal mol^{-1} lower than the value obtained from an iodination kinetics study.

Introduction

Accurate thermochemical information for free-radical intermediates is essential to analysis of reaction mechanisms in complex chemical systems. One experimental approach which can be employed to obtain thermochemical parameters for a radical involves measurement of temperature-dependent rate coefficients for the pair of reactions $\text{RH} + \text{R}' \leftrightarrow \text{R}'\text{H} + \text{R}$; the ideal reaction pair for such a study is one where the heats of formation and absolute entropies of R' , $\text{R}'\text{H}$, and RH are well-characterized and where kinetic data for the two reactions can be obtained over the same temperature range.

In this paper we report the results of temperature-dependent kinetics studies of the following pair of reactions:



The kinetic results have been employed to derive a value for the heat of formation of the CH_3SCH_2 radical, an intermediate in the oxidation of the important atmospheric reduced sulfur compound dimethyl sulfide (CH_3SCH_3).¹

Experimental Technique

The experimental approach involved coupling reactant radical (i.e., Br or CH_3SCH_2) production by 266-nm laser flash photolysis of suitable precursors with time-resolved detection of ground-state bromine atom disappearance or appearance by atomic resonance fluorescence spectroscopy. A schematic diagram of the apparatus, as configured for bromine atom detection, can be found elsewhere,² as can a detailed description of the experimental

methodology.³ Only those aspects of the experimental approach which are unique to this study are discussed below.

Because the temperature range of this study (386–604 K) was higher than in our previous studies of bromine atom kinetics,^{2–4} a different reaction cell was employed. The cell was constructed of quartz and had an internal volume of about 200 cm^3 . A diagram showing the geometry of the reaction cell as well as a discussion of heating and temperature measurement techniques is published elsewhere.⁵

To avoid accumulation of photolysis or reaction products, all experiments were carried out under "slow flow" conditions. The concentration of each component in the reaction mixtures was determined from measurements of the appropriate mass flow rates and the total pressure. The excess reactant (i.e., CH_3SCH_3 or HBr) concentrations were also determined *in situ* in the slow flow system by UV photometry using a 2-m absorption cell. The monitoring wavelengths employed were 228.8 nm for CH_3SCH_3 (Cd line) and 202.6 nm for HBr (Zn^+ line); absorption cross sections used to convert measured absorbances to concentrations were $1.16 \times 10^{-18} \text{ cm}^2$ for CH_3SCH_3 ⁶ and $1.02 \times 10^{-18} \text{ cm}^2$ for HBr.⁴ Since it was normally the case that more than one species in the reaction mixture absorbed at the monitoring wavelength, the excess reagent concentration was usually measured upstream from the photolyte addition point; dilution factors required to correct the measured concentration to the actual reactor concentration never exceeded 1.1.

The gases used in this study had the following stated minimum purities: N_2 , 99.999%; H_2 , 99.999%; HBr, 99.997% (liquid phase in cylinder); Cl_2CO , 99.0% (liquid phase in cylinder). Liquid samples were purchased from Aldrich and had the following stated purities: CH_3SCH_3 , 99+%; CF_2Br_2 , 99%. Nitrogen and hydrogen were used as supplied while HBr, Cl_2CO , CH_3SCH_3 , and CF_2Br_2 were degassed at 77 K before being used to prepare gaseous mixtures with N_2 .

Results

In our study of reaction 1, bromine atoms were generated by 266-nm laser flash photolysis of CF_2Br_2 ($[\text{CF}_2\text{Br}_2]$ ranged from

[†] Georgia Tech Research Institute.

[‡] Present address: National Center for Atmospheric Research, Boulder, CO 80307.

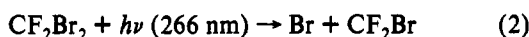
[§] School of Chemistry and Biochemistry.

[⊥] School of Earth and Atmospheric Sciences.

* To whom correspondence should be addressed.

⊙ Abstract published in *Advance ACS Abstracts*, July 1, 1994.

2.3×10^{13} to 2.7×10^{14} molecules cm⁻³):

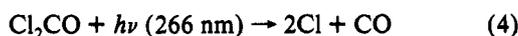


The CF₂Br₂ absorption cross section at 266 nm is approximately 8×10^{-20} cm² while the quantum yield for Br production from CF₂Br₂ photolysis increases from unity at $\lambda = 248$ nm to approximately 2 at $\lambda = 193$ nm.¹⁰ Presumably, at $\lambda \geq 248$ nm, CF₂Br₂ photodissociates as indicated in reaction 2 with unit yield. To ensure rapid relaxation of any photolytically generated Br(²P_{1/2}), about 1 Torr of H₂ was added to the reaction mixture. The reaction

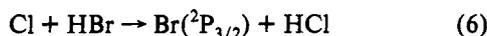


is known to be fast with $k_3 \approx 6 \times 10^{-12}$ cm³ molecule⁻¹ s⁻¹.¹¹

In our study of reaction -1, CH₃SCH₂ radicals were generated as follows:



Reaction 5 is known to occur at a gas kinetic rate,^{12,13} and channel 5a is dominant under the relatively high-temperature, low-pressure conditions employed in this study.¹³ Typical concentrations of Cl₂CO and CH₃SCH₃ were 1×10^{15} and 5×10^{14} molecules cm⁻³, respectively. The concentration of CH₃SCH₃ was kept sufficiently high that >80% of the photolytically generated Cl reacted with CH₃SCH₃ rather than with HBr ($k_6 = 2.25 \times 10^{-11}$ exp(-400/T) cm³ molecule⁻¹ s⁻¹).¹⁴



On the other hand, the concentration of CH₃SCH₃ was kept sufficiently low that the back-reaction, i.e., reaction 1, had only a minor influence on observed Br(²P_{3/2}) kinetics. The Cl₂CO absorption cross section at 266 nm is approximately 2.3×10^{-20} cm²,^{15,16} while the quantum yield for Cl₂CO photodissociation at 253.7 nm has been shown to be unity.¹⁷ Reaction 4 actually occurs in a two-step process involving a ClCO intermediate. However, even in the unlikely event that ClCO is produced without internal excitation, the ClCO lifetime toward decomposition to Cl + CO is short compared to the experimental time scale of 0.1–1 ms.¹⁸

All experiments were carried out under pseudo-first-order conditions with the stable reactant in large excess (factors of 10³–10⁵) over the free-radical reactant. Concentrations of photolytically generated radicals were typically around 3×10^{11} cm⁻³, although this experimental parameter was varied over a wide range (factor of 30). For both reactions studied, observed kinetics were found to be independent of the photolytic precursor concentration(s) and the concentration of photolytically generated radicals. Observed kinetics were also found to be independent of the linear flow rate of the reaction mixture through the reactor and the photolysis laser repetition rate.

In the absence of side reactions which regenerate or deplete the Br(²P_{3/2}) atom concentration, the observed Br(²P_{3/2}) temporal profile following the laser flash in studies of reaction 1 would be described by the relationship

$$\ln(S_0/S_t) =$$

$$\ln\{[\text{Br}]_0/[\text{Br}]_t\} = (k_1[\text{CH}_3\text{SCH}_3] + k_7)t \equiv k't \quad (1)$$

In the above relationship S_0 and S_t are the signal levels immediately after the laser fires and at some later time t , $[\text{Br}]_0$ and $[\text{Br}]_t$ are the bromine atom concentrations corresponding to S_0 and S_t , and

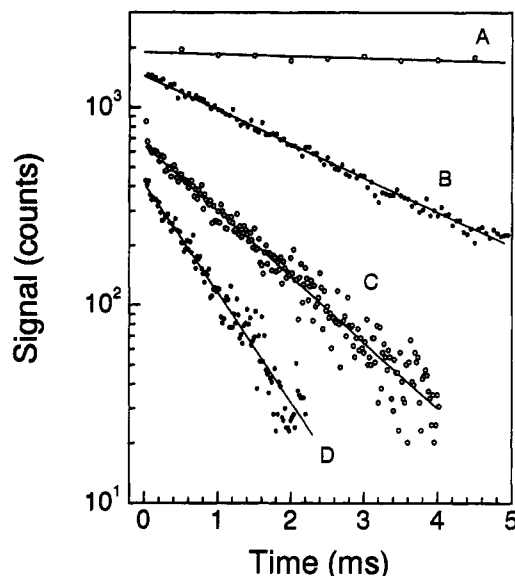
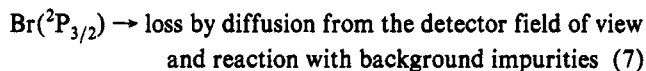


Figure 1. Typical Br(²P_{3/2}) atom temporal profiles observed in the study of reaction 1. Experimental conditions: $P = 50$ Torr, $T = 486$ K, $[\text{H}_2] = 1.3 \times 10^{16}$ molecules cm⁻³, $[\text{CF}_2\text{Br}_2] = 8.0 \times 10^{13}$ molecules cm⁻³, $[\text{Br}(\text{}^2\text{P}_{3/2})]_0 = 1.8 \times 10^{11}$ atoms cm⁻³, $[\text{CH}_3\text{SCH}_3]$ in units of 10^{15} molecules cm⁻³ = (A) 0, (B) 0.577, (C) 1.15, and (D) 1.91. The solid lines represent linear least-squares analyses of the data and give the following pseudo-first-order Br(²P_{3/2}) decay rates in units of s⁻¹: (A) 22, (B) 398, (C) 768, and (D) 1272. For clarity curve C is arbitrarily shifted upward.

k_7 is the first-order rate coefficient for the loss of Br atoms without CH₃SCH₃ present.



The bimolecular rate coefficients of interest, $k_1(T,P)$, are determined from the slopes of k' versus $[\text{CH}_3\text{SCH}_3]$ plots. Observation of Br(²P_{3/2}) temporal profiles which are exponential (i.e., obey eq 1), linear dependencies of k' on $[\text{CH}_3\text{SCH}_3]$, and invariance of observed kinetics to variations in laser photon fluence and photolytic concentration strongly suggests that reactions 1 and 7 are the only processes which effect the Br(²P_{3/2}) time history, although reactions of Br(²P_{3/2}) with impurities in the CH₃SCH₃ sample are not ruled out by the above set of observations. Typical Br(²P_{3/2}) temporal profiles and a typical k' versus $[\text{CH}_3\text{SCH}_3]$ plot observed in our study of reaction 1 are shown in Figures 1 and 2. Kinetic data for reaction 1 are summarized in Table 1.

In the absence of side reactions that remove or produce Br(²P_{3/2}), the observed Br(²P_{3/2}) temporal profile following the laser flash in our study of reaction -1 can be described by the relationship

$$S(t) = a_1 \exp(-r_1 t) + a_2 \exp(-r_2 t) + a_3 \exp(-r_3 t) \quad (II)$$

where it can be shown that

$$r_1 = 0.5\{J_B + J_R + D\} \quad (III)$$

$$r_2 = 0.5\{J_B + J_R - D\} \quad (IV)$$

$$r_3 = k'_5 + k'_6 + k_9 \quad (V)$$

$$a_1 = -(r_3 - r_2)a_3 + (r_2 - J_B)X + k'_{-1}Y + k'_6\{D \quad (VI)$$

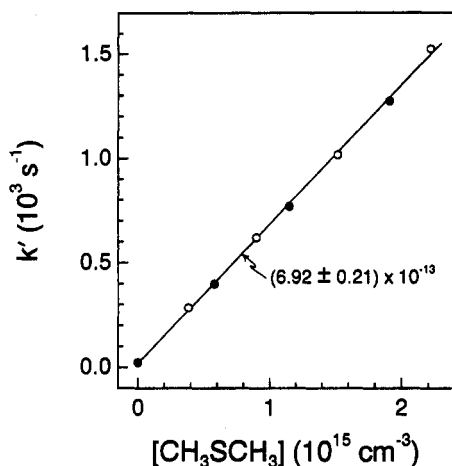


Figure 2. Typical plot of k' versus $[\text{CH}_3\text{SCH}_3]$ observed in the studies of reaction 1. The four closed circles are the data points obtained from the temporal profiles shown in Figure 1. The solid line is obtained from a linear least-squares analysis and gives the bimolecular rate coefficient shown in the figure in units of $\text{cm}^3 \text{ molecule}^{-1} \text{ s}^{-1}$.

TABLE 1: Summary of Kinetic Data for the Reaction $\text{Br}(^2\text{P}_{3/2}) + \text{CH}_3\text{SCH}_3 \rightarrow \text{HBr} + \text{CH}_3\text{SCH}_2^a$

T	P	no. of expts ^b	$[\text{CH}_3\text{SCH}_3]_{\text{max}}$	range of k'	$k_1 \pm 2\sigma^c$
386	50	19	3.70	10–687	1.85 ± 0.05
409	50	11	8.44	37–636	0.716 ± 0.029^d
417	50	5	4.19	13–1339	3.14 ± 0.15
428	50	7	2.82	13–899	3.16 ± 0.07
483	50	6	2.49	18–1556	6.13 ± 0.11
486	50	8	2.22	17–1546	6.92 ± 0.21
487	200	6	2.60	7–1684	6.50 ± 0.30
487	20	5	1.57	21–1177	7.31 ± 0.24
548	50	10	2.40	39–2690	11.0 ± 0.3
604	50	14	1.51	25–2618	17.9 ± 1.1

^a Units are T (K), P (Torr), $[\text{CH}_3\text{SCH}_3]$ ($10^{15} \text{ molecules cm}^{-3}$), k' (s^{-1}), and k_1 ($10^{-13} \text{ cm}^3 \text{ molecule}^{-1} \text{ s}^{-1}$). ^b Expt = measurement of a single pseudo-first-order $\text{Br}(^2\text{P}_{3/2})$ decay rate. ^c Errors represent precision only. ^d Reactant is CD_3SCD_3 .

$$a_2 = \{(r_3 - r_1)a_3 + (r_1 - J_B)X + k'_{-1}Y + k'_6\}/D \quad (\text{VII})$$

$$a_3 = \{k'_6(J_R - r_3) + k'_{-1}k'_5\}/\{(J_B - r_3)(J_R - r_3) - k'_{-1}k'_{-1}\} \quad (\text{VIII})$$

where

$$k'_i = k_i[\text{CH}_3\text{SCH}_3], i = 1, 5 \quad (\text{IX})$$

$$k'_j = k_j[\text{HBr}], j = -1, 6 \quad (\text{X})$$

$$J_B = k'_1 + k_7 \quad (\text{XI})$$

$$J_R = k'_{-1} + k_8 \quad (\text{XII})$$

$$D = \{(J_B - J_R)^2 + 4k'_1k'_{-1}\}^{1/2} = r_1 - r_2 \quad (\text{XIII})$$

$$X = [\text{Br}]_0/[\text{Cl}]_0 \quad (\text{XIV})$$

$$Y = [\text{CH}_3\text{SCH}_2]_0/[\text{Cl}]_0 \quad (\text{XV})$$

and k_8 and k_9 are first-order rate coefficients for the processes

$\text{CH}_3\text{SCH}_2 \rightarrow$ loss by diffusion from the detector field of view and reaction with background impurities (8)

$\text{Cl} \rightarrow$ loss by diffusion from the detector field of view and reaction with background impurities (9)

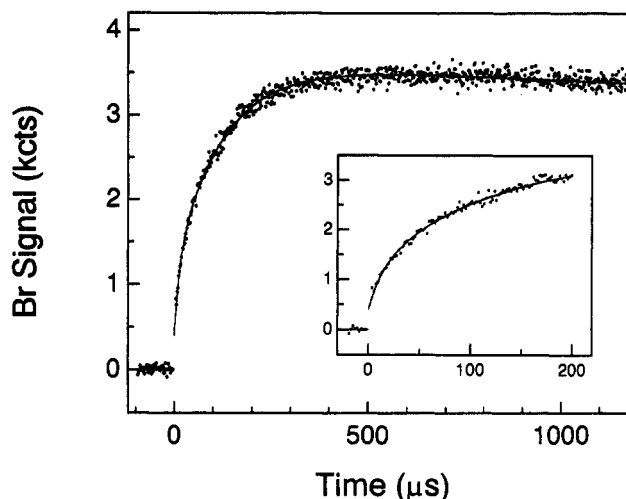


Figure 3. Typical $\text{Br}(^2\text{P}_{3/2})$ atom temporal profile observed in the studies of reaction -1. Experimental conditions: $P = 25$ Torr, $T = 525$ K, $[\text{H}_2] = 5.66 \times 10^{15} \text{ molecules cm}^{-3}$, $[\text{Cl}_2\text{CO}] = 4.24 \times 10^{14} \text{ molecules cm}^{-3}$, $[\text{CH}_3\text{SCH}_3] = 3.53 \times 10^{14} \text{ molecules cm}^{-3}$, $[\text{Cl}]_0 \approx 5 \times 10^{11} \text{ atoms cm}^{-3}$, and $[\text{HBr}] = 1.83 \times 10^{15} \text{ molecules cm}^{-3}$. The solid curve represents a nonlinear least-squares fit of the data to eq II and gives the following best fit parameters: $a_1 = -2445$ cts, $a_2 = 3618$ cts, $a_3 = -769$ cts, $r_1 = 8167 \text{ s}^{-1}$, and $r_2 = 60 \text{ s}^{-1}$. The parameter r_3 was held fixed at $72\,080 \text{ s}^{-1}$. The time-independent background of 1357 cts (measured immediately prior to the laser flash) has been subtracted from each data point.

It should be noted that

$$r_1 + r_2 = J_B + J_R = k'_1 + k_7 + k_8 + k_{-1}[\text{HBr}] \quad (\text{XVI})$$

Hence, for data obtained with the CH_3SCH_3 concentration held constant, a plot of $r_1 + r_2$ versus $[\text{HBr}]$ should be linear with slope $= k_{-1}$.

In the above equations, it is assumed that $k_5 = k_{5a}$; this assumption is approximately correct in the temperature and pressure regime of our study and is employed only to simplify the mathematics; i.e., the determination of k_{-1} does not critically depend on its validity. A nonlinear least-squares analysis of each experimental temporal profile was employed to determine r_1 , r_2 , a_1 , a_2 , and a_3 . Because k_5 and k_6 are well-known and k_9 is negligible compared to $k'_5 + k'_6$, r_3 was not treated as a variable in the fitting procedure. Under typical experimental conditions, r_3 was considerably larger than $r_1 + r_2$, a requirement for accurate evaluation of $r_1 + r_2$. The bimolecular rate coefficients of interest, $k_{-1}(P, T)$, were determined from the slopes of plots of $r_1 + r_2$ versus $[\text{HBr}]$ for data obtained with $[\text{CH}_3\text{SCH}_3]$ held constant (see eq XVI). It should be noted that accurate determination of k_{-1} in these experiments requires that the concentrations of CH_3SCH_3 and HBr be chosen with care. We require that $k'_{-1} \gg k'_1$ (at least for the larger HBr concentrations employed) so that the dominant contribution to $r_1 + r_2$ is from reaction -1, not from reaction 1.

Similar to the situation discussed above for the study of reaction 1, observation of $\text{Br}(^2\text{P}_{3/2})$ temporal profiles that obey eq II, linear dependencies of $r_1 + r_2$ on $[\text{HBr}]$, and invariance of $r_1 + r_2$ to variation in laser photon fluence and photolyte concentration suggests that reactions 1, -1, and 5–9 are the only processes other than possible impurity reactions which significantly affect the $\text{Br}(^2\text{P}_{3/2})$ time history. A typical $\text{Br}(^2\text{P}_{3/2})$ appearance temporal profile and a typical plot of $r_1 + r_2$ versus $[\text{HBr}]$ observed in our study of reaction -1 are shown in Figures 3 and 4. Kinetic data for reaction -1 are summarized in Table 2, while best-fit values of r_1 , r_2 , a_1 , a_2 , and a_3 for data obtained at four representative temperatures are presented in Table 3.

Listed in Table 2 are values of the intercept of the $r_1 + r_2$ versus $[\text{HBr}]$ plots from each temperature. As can be seen from eq XVI, this intercept is the sum of three terms, i.e., k'_1 , k_7 , and k_8 .

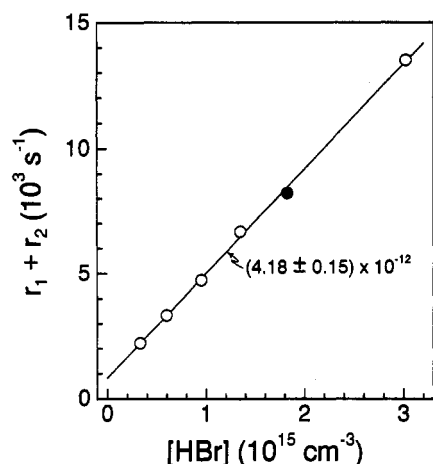
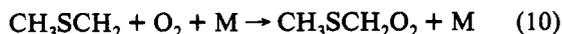


Figure 4. Typical plot of $r_1 + r_2$ versus $[\text{HBr}]$ observed in the studies of reaction -1. The closed circle is the data point obtained from the temporal profile shown in Figure 3. The solid line is obtained from a linear least-squares analysis and gives the bimolecular rate coefficient shown in the figure in units of $\text{cm}^3 \text{molecule}^{-1} \text{s}^{-1}$.

Since $[\text{CH}_3\text{SCH}_3]$ is a known experimental parameter, k'_1 can be subtracted from each intercept, yielding k_d ($\equiv k_7 + k_8$). In our study of $k_1(T)$ the observed background loss of $\text{Br}(^2\text{P}_{3/2})$ was always quite small, i.e., $k_7 < 40 \text{ s}^{-1}$; therefore, the values of k_d listed in Table 2 are dominated by k_8 . It can be seen from Table 2 that k_d systematically decreases as the temperature increases. A likely explanation for the apparently large background loss of $[\text{CH}_3\text{SCH}_2]$ is the presence of O_2 impurity possibly due to small leaks or the porosity of the Teflon tubing used in the flow system.



A room temperature value of $5.7 \times 10^{-12} \text{ cm}^3 \text{molecule}^{-1} \text{s}^{-1}$ has been reported for k_{10} in 1 atm of SF_6 .¹⁹ Hence, O_2 levels in the 10 mTorr range could account for our observed values for k_d (Table 2). In any event the value of the intercept was never more than 25% and typically less than 10% of the maximum value of $r_1 + r_2$ at any temperature. We therefore conclude that the chemistry contributing to the intercept did not significantly impact the accuracy of our measurement of $k_{-1}(T)$.

As indicated in Tables 1 and 2, pressure dependence studies were carried out for reactions 1 and -1; as expected, no evidence for pressure-dependent rate coefficients was observed over the range investigated (20–200 Torr for reaction 1; 10–50 Torr for reaction -1). Arrhenius plots for reactions 1 and -1 are shown in Figure 5. The solid lines in Figure 5 are obtained from linear least-squares analyses of the $\ln k_{\pm 1}$ versus T^{-1} data; these analyses give the following Arrhenius expressions in units of $\text{cm}^3 \text{molecule}^{-1} \text{s}^{-1}$:

$$k_1 = (9.0 \pm 2.9) \times 10^{-11} \exp[(-2386 \pm 151)/T]$$

$$k_{-1} = (8.6 \pm 2.5) \times 10^{-13} \exp[(836 \pm 140)/T]$$

Errors in the above expressions are 2σ and represent precision only. On the basis of observed precision and consideration of possible systematic errors (see below), we estimate the absolute accuracy of each measured bimolecular rate coefficient to be $\pm 15\%$ for $k_1(T)$ values and $\pm 25\%$ for $k_{-1}(T)$ values.

As discussed briefly above, a number of potential systematic errors in our kinetic measurements can be ruled out based on the observed invariance of $\text{Br}(^2\text{P}_{3/2})$ temporal profiles to variations in laser photon fluence, photolyte concentrations, flow velocity through the reactor, and laser pulse repetition rate; these include contributions to $\text{Br}(^2\text{P}_{3/2})$ kinetics from radical-radical side reactions, from radical-photolyte side reactions, from reactions involving radicals which are produced by reactant photolysis, or

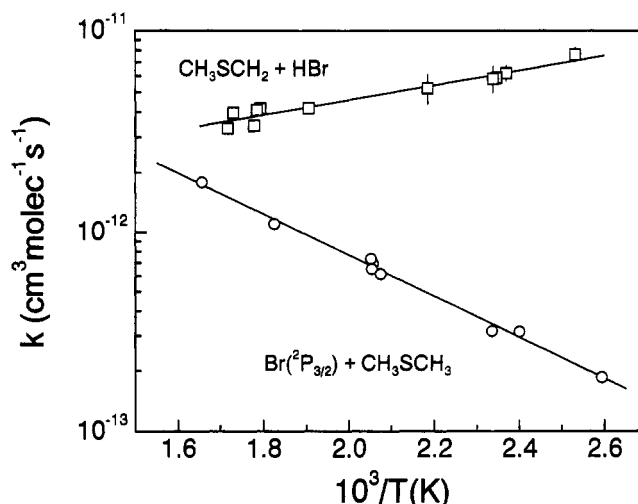


Figure 5. Arrhenius plots for reactions 1 and -1. Solid lines are obtained from linear least-squares analyses which yield the Arrhenius expressions given in the text.

from reactions involving stable products which build up in concentration with successive laser flashes. *In situ* measurements of stable reactant (i.e., CH_3SCH_3 and HBr) concentrations greatly reduce another potential source of systematic error.

One type of kinetic interference which needs to be addressed is the potential contribution to measured rate coefficients from impurity reactions. The relatively unreactive nature of Br atoms makes it unlikely that impurity reactions were a problem in our study of reaction 1. The most likely impurity problem in our study of reaction -1 is from Br_2 . Potential sources of Br_2 are impurity in the HBr sample and residual Br_2 from heterogeneous reactions of HBr (presumably on metal surfaces of valves and fittings). There is no kinetic data in the literature for reaction 11.



However, based on reported rate coefficients for reactions of Br_2 with alkyl radicals²⁰ and thyl radicals,^{3,21} it seems safe to assume that reaction 11 proceeds at a near gas kinetic rate. Since CH_3SCH_2 probably reacts with Br_2 10–50 times faster than with HBr , the HBr concentration must be several hundred times larger than the Br_2 concentration before Br_2 interferences can be considered unimportant. To investigate the Br_2 interference problem, a 2-m absorption cell was positioned in the slow flow system downstream from the reaction cell and employed to monitor Br_2 photometrically (at 404.7 nm) with typical $\text{Cl}_2\text{CO}/\text{CH}_3\text{SCH}_3/\text{HBr}/\text{H}_2/\text{N}_2$ mixtures flowing through the system. No absorption was observed (i.e., $I/I_0 > 0.998$) even at HBr levels as high as $5 \times 10^{16} \text{ molecules cm}^{-3}$. Since the Br_2 absorption cross section at 404.7 nm is about $6 \times 10^{-19} \text{ cm}^2$,²² these experiments suggest that $[\text{Br}_2] < 0.0004[\text{HBr}]$.

CH_3SCH_3 has a small absorption cross section at 266 nm ($1.2 \times 10^{-21} \text{ cm}^2$).²³ An interference in our measurement of k_{-1} would be present if a significant fraction of the observed Br atom appearance were due to reaction of CH_3SCH_3 photoproducts (rather than CH_3SCH_2) with HBr . As discussed above, the Cl atom photolyte, Cl_2CO , has an absorption cross section at 266 nm of $2.3 \times 10^{-20} \text{ cm}^2$ ^{15,16} with an effective Cl atom yield of 2.^{17,18} All experiments to measure k_{-1} were carried out with $[\text{Cl}_2\text{CO}]$ greater than or equal to $[\text{CH}_3\text{SCH}_3]$. The concentration of any CH_3SCH_3 photofragments were therefore never more than $\sim 5\%$ of the initial $[\text{Cl}]$, and since both CH_3S and CH_3 react more slowly with HBr than does CH_3SCH_3 (see ref 3 and the discussion in the next paragraph), it is concluded that CH_3SCH_3 photolysis did not represent a significant systematic error in our measurements. In our measurements of k_1 , CH_3SCH_3 photo-

TABLE 2: Summary of Kinetic Data for the Reaction $\text{HBr} + \text{CH}_3\text{SCH}_2 \rightarrow \text{Br}(^2\text{P}_j) + \text{CH}_3\text{SCH}_3^a$

<i>T</i>	<i>P</i>	no. of expts ^b	range of [HBr]	range of (<i>r</i> ₁ + <i>r</i> ₂) ^c	intercept ^d	<i>k</i> _d ^e	<i>k</i> ₋₁ ± 2σ ^f
395	10, 25, 50	8	4.19–36.8	6803–32840	3770	3250	7.67 ± 0.60
422	25	4	6.59–15.1	7132–12810	3300	3130	6.21 ± 0.55
426	25	5	4.13–21.9	5212–15640	2700	2420	5.90 ± 0.12
428	25	5	3.24–20.7	4784–15030	3060	2870	5.85 ± 0.87
458	25	5	1.93–25.0	3211–14750	2350	2150	5.25 ± 0.87
525	25	6	3.32–30.2	2222–13510	820	470	4.18 ± 0.15
558	25	5	3.32–18.6	2738–9142	1350	830	4.17 ± 0.13
561	25	5	5.17–18.1	3681–8943	1450	925	4.09 ± 0.23
563	25	6	3.73–23.4	2798–11180	1500	944	3.43 ± 0.09
578	25	6	2.81–18.3	2526–8690	1310	700	3.96 ± 0.23
583	10, 25, 50	11	1.71–30.7	1997–11450	1570	960	3.33 ± 0.13

^a Units are *T* (K), *P* (Torr), [HBr] (10¹⁴ molecules cm⁻³), *r*₁ + *r*₂ (s⁻¹), intercept (s⁻¹), *k*_d (s⁻¹), and *k*₋₁ (10⁻¹² cm³ molecule⁻¹ s⁻¹). ^b Expt = measurement of a single Br(²P_{3/2}) temporal profile. ^c *r*₁ + *r*₂ defined in eq XVI. ^d Intercept of (*r*₁ + *r*₂) versus [HBr] plot. ^e *k*_d = background radical loss rate (see text). ^f Errors represents precision only.

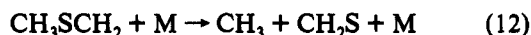
TABLE 3: Experimental Conditions and Best Fit Parameters at Four Representative Temperatures Obtained from Observation and Analysis of Br(²P_{3/2}) Temporal Profiles Observed following 266-nm Laser Flash Photolysis of Cl₂CO/H₂/CH₃SCH₃/HBr/N₂ Mixtures

temp, K	total press.	[H ₂]	[Cl ₂ CO]	[CH ₃ SCH ₃]	[HBr]	<i>a</i> ₁	<i>r</i> ₁	<i>a</i> ₂	<i>r</i> ₂	<i>a</i> ₃	<i>r</i> ₃ ^b
395	10.0	237	15.5	11.2	4.19	-637	8023	822	221	258	208 400
	47.3	89	5.90	4.12	5.56	-1693	6810	1927	-7.2	-44	80 200
	24.2	124	8.17	5.88	5.64	-1613	8045	1830	56	131	112 600
	25.0	125	8.36	5.77	10.9	-1669	11880	1878	24	186	114 900
	24.6	120	7.40	5.59	15.8	-1329	16060	1618	-0.5	-119	115 600
	24.7	80	7.38	5.31	23.6	-1845	22530	2104	-23	167	116 800
	10.3	135	8.65	6.42	32.7	-1256	27430	1540	48	-26	114 500
	25.6	107	6.83	5.13	36.8	-1555	32870	1892	-29	-164	124 100
458	23.0	699	4.36	4.39	1.93	-872	3108	1034	68	92	73 880
	23.6	691	4.31	4.26	6.91	-1489	5725	1660	56	134	76 410
	23.5	662	4.13	4.08	11.7	-1459	8353	1636	49	91	77 950
	24.1	647	4.04	3.92	17.9	-983	12840	1187	34	11	81 080
	25.0	636	3.97	3.85	25.0	-1361	14730	1739	23	-61	86 710
525	24.5	630	4.73	3.89	3.32	-3483	2156	4049	66	-195	61 730
	24.4	614	4.54	3.79	5.98	-3282	3268	3994	71	-465	62 980
	25.1	607	4.54	3.78	9.52	-3017	4668	3819	67	-537	66 680
	25.1	586	4.38	3.72	13.5	-2758	6612	3725	61	-694	69 850
	25.3	566	4.24	3.53	18.3	-2445	8167	3618	60	-769	72 080
	26.1	525	3.93	3.33	30.1	-1979	13460	3445	46	-1051	81 600
578	24.9	113	9.42	4.39	2.81	-1875	2429	2303	97	-188	65 350
	25.0	111	9.17	4.41	4.60	-1695	3025	2139	102	-272	67 560
	25.1	105	8.78	4.24	7.67	-1465	4123	2004	91	-470	68 640
	25.2	107	8.93	4.17	9.66	-1873	5126	2536	97	-490	69 840
	24.9	105	8.48	3.96	13.4	-1804	6336	2605	95	-618	71 060
25.1	96	8.08	3.86	18.3	-1666	8606	2541	84	-565	75 180	

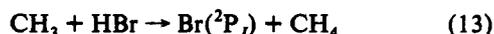
^a Units are pressure (Torr), concentrations (10¹⁴ molecules cm⁻³), *a*_{*i*} (signal counts), and *r*_{*i*} (s⁻¹). ^b This parameter was fixed during the regression analysis (see text).

products could only interfere via radical-radical reactions that would affect the atomic bromine concentration. Under the conditions of our experiments the amount of CH₃SCH₃ photolyzed (a maximum of 3 × 10¹⁰ molecules cm⁻³) was small enough that radical-radical reactions would not occur on the time scale for Br(²P_{3/2}) loss via reaction with CH₃SCH₃.

Another potential systematic error in our study of reaction -1 centers around the possible occurrence of the reaction



Using the CH₃SCH₂ heat of formation determined in this study (see below) in conjunction with the best available heats of formation for CH₃²⁴ and CH₂S²⁵⁻²⁷ leads to the conclusion that the H₃C-SCH₂ bond strength is 30 ± 3 kcal mol⁻¹. Hence, it is conceivable that, near the high-temperature end of our range of experimental conditions (i.e., *T* ~ 600 K), reaction 12 could occur rapidly enough that the rate-limiting step in production of bromine atoms was not reaction -1, but rather reaction 13.



To examine this possibility, we have directly measured *k*₁₃ at 573 K by monitoring Br(²P_{3/2}) appearance following 266-nm laser

flash photolysis of Cl₂CO/CH₄/HBr/H₂/N₂ mixtures, i.e., using the Cl + CH₄ reaction as a source of methyl radicals. A plot of *r*₁ + *r*₂ versus [HBr] for this experiment is shown in Figure 6; the slope, (2.09 ± 0.13) × 10⁻¹² cm³ molecule⁻¹ s⁻¹, is *k*₁₃(573 K). This value agrees well with the value 2.04 × 10⁻¹² cm³ molecule⁻¹ s⁻¹ obtained via extrapolation of the Arrhenius expression we report elsewhere,⁴ which is based on kinetics studies carried out over the temperature range 257–422 K (*k*₁₃ = 1.3 × 10⁻¹² exp(-233/*T*) cm³ molecule⁻¹ s⁻¹). When CH₃SCH₃ was employed in the reaction mixtures instead of CH₄, a significantly faster value, *k*(573 K) ~ 3.7 × 10⁻¹² cm³ molecule⁻¹ s⁻¹, was obtained for the "apparent" rate coefficient (see Figure 5). This observation, coupled with the fact that the "apparent" activation energy (i.e., the slope of the ln *k* versus *T*⁻¹ plot) did not change as a function of temperature, leads to the conclusion that reactions 12 and 13 were not a significant interference in our study of reaction -1.

Another possible interference in our measurement of *k*₋₁(*T*) results from the presence of H₂ which was added to ensure that any atomic bromine formed in the ²P_{1/2} state was rapidly quenched to the ²P_{3/2} ground state. At the higher end of our temperature range the reaction



becomes rapid enough to be significant.²⁸ The hydrogen atom

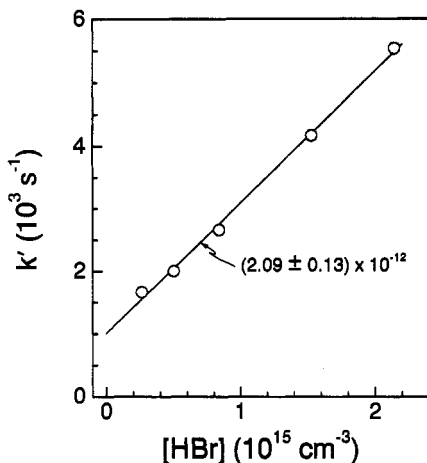


Figure 6. Plot of k' versus $[\text{HBr}]$ observed in the study of reaction 13. Experimental conditions: $T = 573 \text{ K}$, $P = 25 \text{ Torr}$, $[\text{H}_2] = 1.0 \times 10^{16} \text{ molecules cm}^{-3}$, $[\text{Cl}_2\text{CO}] = 9.1 \times 10^{14} \text{ molecules cm}^{-3}$. The solid line represents a linear least-squares analysis of the data which gives the bimolecular rate coefficient shown in the figure in units of $\text{cm}^3 \text{ molecule}^{-1} \text{ s}^{-1}$.

will then quickly react with HBr^{29}



In order to access the contribution of this additional Br production process, we simulated the chemistry under typical experimental conditions at 583 K using a numerical integration routine. The reaction mechanism included reactions ± 1 , 5–9, and 14–16.

H \rightarrow loss by diffusion from the detector field of view and reaction of background impurities (16)

Simulated Br time dependencies were generated at several typical levels of $[\text{HBr}]$ and at constant $[\text{CH}_3\text{SCH}_3]$. Each simulated Br temporal profile was then subjected to the same nonlinear least-squares fitting routine as was used in analyses of the experimental data. The slope of the resulting $r_1 + r_2$ versus $[\text{HBr}]$ plot was $\approx 3\%$ lower when $[\text{H}_2] = 0$ than when $[\text{H}_2]$ was set to the experimental value of $6 \times 10^{15} \text{ molecules cm}^{-3}$. Since this simulation was carried out under conditions where the contribution of reactions 14 and 15 would be greatest, no corrective action was deemed necessary to account for this minor interference.

Discussion

Reaction Mechanisms. Since we wish to employ our kinetic data to evaluate thermochemistry, the identity of the reaction products is a crucial issue. Can we be sure that $\text{Br}({}^2\text{P}_{3/2}) + \text{CH}_3\text{SCH}_3$ produces $\text{CH}_3\text{SCH}_2 + \text{HBr}$ with unit yield, and can we be sure that $\text{CH}_3\text{SCH}_2 + \text{HBr}$ produces $\text{Br}({}^2\text{P}_{3/2}) + \text{CH}_3\text{SCH}_3$ with unit yield? In the case of the $\text{Br}({}^2\text{P}_{3/2}) + \text{CH}_3\text{SCH}_3$ reaction, we have found that addition to the sulfur atom is the dominant reaction pathway at $T \leq 300 \text{ K}$.³⁰ However, at the temperatures employed in this study, $T \geq 386 \text{ K}$, the adduct lifetime toward unimolecular decomposition back to reactants is so short that its existence is kinetically inconsequential. At temperatures around 400 K, we have obtained strong evidence that the dominant pathway for the $\text{Br}({}^2\text{P}_{3/2}) + \text{CH}_3\text{SCH}_3$ reaction is hydrogen transfer. First, we find that at $T = 409 \text{ K}$ $\text{Br}({}^2\text{P}_{3/2})$ reacts with CD_3SCD_3 a factor of 3.7 more slowly than with CH_3SCH_3 (Table 1); this result strongly suggests that the reaction mechanism involves breaking a carbon–hydrogen bond. Second, in experiments which will be published elsewhere, we have employed time-resolved tunable diode laser absorption spectroscopy to directly monitor HBr production from the $\text{Br}({}^2\text{P}_{3/2}) + \text{CH}_3\text{SCH}_3$ reaction;³¹ using the $\text{Br}({}^2\text{P}_{3/2}) + (\text{CH}_3)_3\text{CH}$ reaction

TABLE 4: Thermochemical Parameters for the Reaction $\text{Br}({}^2\text{P}_{3/2}) + \text{CH}_3\text{SCH}_3 \rightarrow \text{CH}_3\text{SCH}_2 + \text{HBr}$

T, K	$\Delta H_i^a \text{ kcal mol}^{-1}$		$\Delta S_i^a \text{ cal mol}^{-1} \text{ deg}^{-1}$	
	2nd law	3rd law	2nd law	3rd law
470	6.40 ± 0.58	6.67 ± 1.37	9.25 ± 0.40	9.82 ± 1.30
298	5.98 ± 0.58	6.24 ± 1.37	7.83 ± 1.96	8.72 ± 1.30
0	5.24 ± 0.59	5.50 ± 1.38		

^a Errors are 2σ and represent best estimate of absolute accuracy.

as a “unit yield calibration”, we find that the HBr yield from $\text{Br}({}^2\text{P}_{3/2}) + \text{CH}_3\text{SCH}_3$ is near unity. For the $\text{CH}_3\text{SCH}_2 + \text{HBr}$ reaction, qualitative thermochemical considerations suggest that production of $\text{CH}_3\text{SCH}_3 + \text{Br}$ should be the dominant reaction pathway. Observed resonance fluorescence signal levels confirm that atomic bromine is produced with high yield. However, production of electronically excited bromine atoms, $\text{Br}({}^2\text{P}_{1/2})$, is a possibility which warrants consideration.



If the $\text{CH}_3\text{SCH}_2 + \text{HBr}$ reaction proceeded exclusively or a significant fraction of the time via channel $-1'$, then we would be overestimating the rate of the true reverse of reaction 1 and our reported enthalpy change for reaction 1 (see below) would be in error. A simple thermochemical argument based on the measured activation energy for reaction 1 can be used to place a reasonable upper limit on $k_{-1'}$. It is reasonable to assume that the activation energy for reaction $-1'$ is greater than $-2.0 \text{ kcal mol}^{-1}$. Since the bromine atom spin–orbit splitting is $10.5 \text{ kcal mol}^{-1}$, reaction $-1'$ must be endothermic by at least $3.7 \text{ kcal mol}^{-1}$, i.e., $10.5 - 2.0 - 4.8 \text{ kcal mol}^{-1}$ where $4.8 \text{ kcal mol}^{-1}$ is the measured activation energy for reaction 1. Taking $1 \times 10^{-11} \text{ cm}^3 \text{ molecule}^{-1} \text{ s}^{-1}$ as an upper limit A factor for reaction $-1'$ (a polyatomic + diatomic reaction) and $3.7 \text{ kcal mol}^{-1}$ as a lower limit activation energy for reaction $-1'$ leads to the result $k_{-1'} \leq 9.0 \times 10^{-14} \text{ cm}^3 \text{ molecule}^{-1} \text{ s}^{-1}$ at 395 K and $k_{-1'} \leq 4.1 \times 10^{-13} \text{ cm}^3 \text{ molecule}^{-1} \text{ s}^{-1}$ at 583 K; comparison of these limits with the rate coefficients reported in Table 2 shows that upper limit branching ratios for formation of $\text{Br}({}^2\text{P}_{1/2})$ are 0.013 at 395 K and 0.11 at 583 K. We conclude that it is safe to ignore the possible occurrence of reaction $-1'$ in our thermochemical analysis.

Thermochemistry. From the Arrhenius parameters determined in this study, we can obtain the enthalpy change and entropy change associated with reaction 1. One approach, the “second law method”, employs the following relationships to obtain thermochemical parameters:

$$\Delta H_1 = E_1 - E_{-1} \quad (\text{XVII})$$

$$\Delta S_1 = R \ln(A_1/A_{-1}) \quad (\text{XVIII})$$

where ΔH_i , ΔS_i , E_i , and A_i are the enthalpy change, entropy change, activation energy, and A factor for reaction i . Thermochemical parameters for reaction 1 obtained from the second law analysis are tabulated in Table 4. The temperature 470 K is the arithmetic mean of the T^{-1} ranges employed in the determinations of $k_1(T)$ and $k_{-1}(T)$. Values of ΔH at 298 and 0 K were computed using heat capacity corrections obtained from the JANAF tables²⁴ for Br and HBr and calculated using the structural information in Table 5 for CH_3SCH_3 and CH_3SCH_2 . Second law values for ΔS at 298 K were computed from the relationship

$$\begin{aligned} \Delta G_{298} &= \Delta H_{298} - T\Delta S_{298} = -RT \ln K_{\text{eq}}(298 \text{ K}) \\ &= RT \ln[k_{-1}(298 \text{ K})/k_1(298 \text{ K})] \end{aligned} \quad (\text{XIX})$$

Values for $k_1(298 \text{ K})$ and $k_{-1}(298 \text{ K})$ were computed from the Arrhenius expressions reported above.

TABLE 5: Structural Parameters Used in the Evaluation of Absolute Entropies and Heat Capacities for CH₃SCH₃ and CH₃SCH₂^a

	CH ₃ SCH ₃ ^b	CH ₃ SCH ₂	symmetry
vibrational frequencies, cm ⁻¹	2998, 2998, 2990, 2970, 2930, 2930, 1444, 1444, 1439, 1430, 1331, 1315, 1030, 973, 940, 903, 743, 695, 282	3157, 3025, 3006, 2997, 2897, 1419, 1407, 1358, 1294, 991, 929, 866, 811, 689, 282, 281 3139, 3010, 3005, 2996, 2896, 1418, 1407, 1357, 1294, 993, 930, 872, 807, 689, 398, 282	C _s C ₁
barriers to internal rotation, kcal mol ⁻¹	V ₀ (CH ₃) = 1.89 ^c (doubly degenerate)	V ₀ (CH ₃) = 1.68 V ₀ (CH ₂) = 1.40–6.15 ^d	
moments of inertia ABC, amu ³ Å ⁶	173180	129724 (C _s) 129976 (C ₁)	
I _r (CH ₃), amu Å ² I _r (CH ₂), amu Å ²	3.24	3.01 1.77	

^a Except where noted otherwise all parameters are from *ab initio* calculations at the UMP2/g-31+G(2d) level³² (see text for further discussion).
^b Experimentally observed values from ref 33. ^c From ref 34. ^d Extremes of suggested barrier heights, the lower from ref 35 and the higher from ref 32; thermochemical parameters calculated at extremes and averaged.

TABLE 6: Comparison of CH₃SCH₂ Thermochemical Results from This Study with Literature Values^a

T, K	ΔH _{f,T}	C–H bond strength in CH ₃ SCH ₂	ref
298	32.7 ± 1.4	93.7 ± 1.4	this work
	35.6 ± 1.0 ^b	96.6 ± 1.0 ^b	35
0	35.3 ± 1.4	92.0 ± 1.4	this work
	34.8 ± 2.5	91 ± 2.5	38
	37.3		39

^a Units are kcal mol⁻¹ for the thermochemical parameters. ^b These values were arrived at using an assumed activation energy for the CH₃SCH₂ + HI reaction of 1.0 ± 0.5 kcal mol⁻¹.

An alternate approach for obtaining thermochemical parameters is the “third law method” where the entropy change is calculated using standard statistical mechanical methods³⁶ and employed in conjunction with an experimental value for K_{eq}(T) to obtain ΔH_T (from eq XIX). Absolute entropies as a function of temperature were obtained from the JANAF tables²⁴ for Br and HBr, and calculated using the structural information in Table 5 for CH₃SCH₃ and CH₃SCH₂. The uncertainty in the third law ΔS value is based on estimated uncertainties in key structural parameters, most notably the low-frequency vibrational modes and internal rotation barriers in CH₃SCH₂. The structural parameters for CH₃SCH₂ listed in Table 5 are based on *ab initio* quantum chemical calculations carried out by McKee.³² His calculated bond angles and bond lengths (for the structure with C₁ symmetry) agree well with those reported in a recent *ab initio* theoretical study by Baker and Dyke.³⁷ McKee finds that two structures with C₁ and C_s symmetry, respectively, are very close in energy. The calculated frequency of the CH₂ wag changes considerably between the two structures; its values (scaled downward by 5% from those actually calculated) are 281 cm⁻¹ (C_s) and 398 cm⁻¹ (C₁). Another major source of uncertainty is the barrier for internal rotation of the CH₂ group. McKee’s calculations suggest that this barrier could be very large (6.15 kcal mol⁻¹) while Shum and Benson³⁵ estimate a barrier of 1.40 kcal mol⁻¹. We have carried out four separate calculations of the absolute entropy of CH₃SCH₂ (S^o) using different pairs of the above values for the CH₂ wag frequency and the barrier to CH₂ internal rotation. Reported heat capacity corrections and third law ΔS values employ the average result with uncertainties adjusted to span the range of reasonable possibilities. The four calculations give S^o values which range from 70.84 to 73.09 cal mol⁻¹ K⁻¹; the average value is 71.89 cal mol⁻¹ K⁻¹.

Values for ΔH_{f,0} and ΔH_{f,298} for CH₃SCH₂, which are given in Table 6, were calculated from our ΔH_{rxn,T} determinations using literature values for the heats of formation of Br,²⁴ HBr,²⁴ and CH₃SCH₃.⁴⁰ Simple averages of the second and third law enthalpies of reaction have been employed to obtain our reported heat of formation; this approach seems reasonable since (a) estimated uncertainties in the second and third law determinations

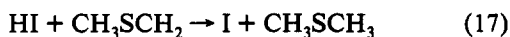
do not differ greatly and (b) the second and third law values for ΔH_{f,T} agree to within a few tenths of a kcal mol⁻¹. The reported uncertainties in ΔH_{f,T} represent 2σ estimates of absolute accuracy; since the 2σ error estimates for the individual second and third law determinations are significantly larger than the deviations of the two determinations from their mean, we take the larger of the (second and third law) error estimates to be the error for the mean. The possible small contribution from reaction -1', i.e., a channel forming Br(²P_{1/2}) (see above), represents an insignificant source of systematic error.

Comparison with Previous Research. To our knowledge there have been no previous kinetics studies of either reaction 1 or -1. The preexponential factor that we observe for reaction 1 is similar to those observed for other atom plus polyatomic hydrogen abstraction reactions. In the case of the reverse process, reaction -1, a significant negative activation energy is observed. It is interesting to note that in recent studies negative activation energies have been observed for reactions of carbon-centered radicals with HBr^{4,41} and HI,⁴² while positive activation energies have been measured for reactions of sulfur-centered radicals with HBr.³ In fact, the Arrhenius parameters reported here for reaction -1 are similar to the Arrhenius parameters for the C₂H₅ + HBr and *t*-C₄H₉ + HBr reactions.^{4,41}

While the experimental evidence for negative activation energies in reactions of carbon-centered radicals with HBr and HI is very strong, the theoretical interpretation of this counterintuitive phenomenon is less clear. Apparently, reaction proceeds via formation of a weakly bound complex. As shown by Mozurkewich and Benson,⁴³ if the transition state leading from reactants to complex (TS1) is loose and the transition state leading from complex to products is both tighter and lower in energy compared to TS1, than a negative activation energy should be observed. McEwen and Golden⁴⁴ have reported a two-channel RRKM calculation that models the *t*-C₄H₉ + HI (DI) reactions as proceeding via formation of a weakly bound (CH₃)₃C...I...H (D) complex. They were able to reproduce the kinetic results of Seetula et al.⁴² for *t*-C₄H₉ + HI with complex binding energies as low as 3 kcal mol⁻¹. Interestingly, their models which are capable of reproducing experimental *k*(T) values for *t*-C₄H₉ + HI also predict an inverse kinetic isotope effect (KIE), i.e., *k*_{HI} < *k*_{DI}; this prediction results from the fact that the transition state leading from complex to products becomes looser with the lower vibrational frequencies associated with deuterium substitution. No experimental determination of the KIE for *t*-C₄H₉ + HI, DI has been reported. However, “normal” kinetic isotope effects are observed for CH₃, C₂H₅, and *t*-C₄H₉ reactions with HBr, i.e., *k*_{HBr} > *k*_{DBr}.⁴ A detailed theoretical study of the CH₃ + HBr reaction, which has an activation energy of about -0.4 kcal mol⁻¹,^{4,45} has been reported by Chen et al.^{46,47} They calculated a potential energy surface at the G1 level of theory and deduced

the existence of a *hydrogen-bridged* complex with C_{3v} symmetry which is bound by 0.28 kcal mol⁻¹ and is formed without activation energy. Chen et al. calculated rate constants for CH₃ + HBr, CH₃ + DBr, and CD₃ + HBr from RRKM theory with corrections for tunneling. By adjusting the height of the barrier toward dissociation to products, they were able to obtain values for *k*(*T*) which agreed fairly well with experiment;^{4,45} furthermore, their calculated isotope effects agreed quantitatively with experiment.⁴

Table 6 contains a comparison of our thermochemical results with previously reported values. Shum and Benson³⁵ reported a value of Δ*H*_{f,298} for CH₃SCH₂ that is approximately 3.0 kcal mol⁻¹ larger than the result reported in this study; these investigators studied the iodination of CH₃SCH₃ at elevated temperatures (630–650 K). Kinetic information was arrived at indirectly by monitoring the rate of change of [I₂] and total pressure. In order to obtain their reported thermochemical results, Shum and Benson assumed a value of 1.0 ± 0.5 kcal mol⁻¹ for the activation energy for the reaction



If the activation energy for reaction 17 is actually negative (as we report for the analogous CH₃SCH₂ + HBr reaction), then the difference between Shum and Benson's value for Δ*H*_f(CH₃SCH₂) and the value reported in this study would be even larger. The only other experimental thermochemical information available in the literature is from a recent molecular beam photofragmentation study of CH₃SCH₃ by Ng and co-workers,³⁸ in which they report a value of 91 ± 2.5 kcal mol⁻¹ for the C–H bond strength in CH₃SCH₃; their result is in good agreement with our reported value of 92.0 ± 1.4 kcal mol⁻¹ although our error limits are nearly a factor of 2 smaller. A recent *ab initio* calculation by Ma et al.³⁹ obtains Δ*H*_{f,0} = 37.3 kcal mol⁻¹, somewhat higher than our value of 35.3 ± 1.4 kcal mol⁻¹ but in agreement within estimated combined uncertainties.

Acknowledgment. We thank S. Wang for assisting with some of the preliminary experiments, M. L. McKee for providing theoretical calculations of structural parameters for CH₃SCH₂, and R. E. Stickel for several helpful discussions. This research was supported by Grant ATM-9104807 from the National Science Foundation and Grant NAGW-1001 from the National Aeronautics and Space Administration.

References and Notes

- Stickel, R. E.; Zhao, Z.; Wine, P. H. *Chem. Phys. Lett.* **1993**, *212*, 312.
- Nicovich, J. M.; Shackelford, C. J.; Wine, P. H. *J. Photochem. Photobiol., A: Chem.* **1990**, *51*, 141.
- Nicovich, J. M.; Kreutter, K. D.; van Dijk, C. A.; Wine, P. H. *J. Phys. Chem.* **1992**, *96*, 2518.
- Nicovich, J. M.; van Dijk, C. A.; Kreutter, K. D.; Wine, P. H. *J. Phys. Chem.* **1991**, *95*, 9890.
- Nicovich, J. M.; Gump, C. A.; Ravishankara, A. R. *J. Phys. Chem.* **1982**, *86*, 1684.
- Wine, P. H.; Kreutter, N. M.; Gump, C. A.; Ravishankara, A. R. *J. Phys. Chem.* **1981**, *85*, 2660.
- Molina, L. T.; Molina, M. J.; Rowland, F. S. *J. Phys. Chem.* **1982**, *86*, 2672.
- Gillotay, D.; Simon, P. C. *J. Atmos. Chem.* **1989**, *8*, 41.
- Burkholder, J. B.; Wilson, R. R.; Gierczak, T.; Talukdar, R.; McKeen, S. A.; Orlando, J. J.; Vaghjiani, G. L.; Ravishankara, A. R. *J. Geophys. Res.* **1991**, *96*, 5025.
- Talukdar, R. K.; Vaghjiani, G. L.; Ravishankara, A. R. *J. Chem. Phys.* **1992**, *96*, 8194.
- Nesbitt, D. J.; Leone, S. R. *J. Chem. Phys.* **1980**, *73*, 6182.
- Nielsen, O. J.; Sidebottom, H. W.; Nelson, L.; Rattigan, O.; Treacy, J. J.; O'Farrell, D. *Int. J. Chem. Kinet.* **1990**, *22*, 603.
- Stickel, R. E.; Nicovich, J. M.; Wang, S.; Zhao, Z.; Wine, P. H. *J. Phys. Chem.* **1992**, *96*, 9875.
- Nicovich, J. M.; Wine, P. H. *Int. J. Chem. Kinet.* **1990**, *22*, 379.
- Heicklen, J. *J. Am. Chem. Soc.* **1965**, *87*, 445.
- Moule, D. C.; Foo, P. D. *J. Chem. Phys.* **1971**, *55*, 1262.
- Okabe, H. *J. Chem. Phys.* **1977**, *66*, 2058.
- Nicovich, J. M.; Kreutter, K. D.; Wine, P. H. *J. Chem. Phys.* **1990**, *92*, 3539.
- Wallington, T. J.; Ellermann, T.; Nielsen, O. J. *J. Phys. Chem.* **1993**, *97*, 8442.
- Timonen, R. S.; Seetula, J. A.; Gutman, D. *J. Phys. Chem.* **1990**, *94*, 3005.
- Fenter, F. F.; Anderson, J. G. *J. Phys. Chem.* **1991**, *95*, 3172.
- Calvert, J. G.; Pitts, J. N., Jr. *Photochemistry*; Wiley: New York, 1966.
- Hearn, C. H.; Turcu, E.; Joens, J. A. *Atmos. Environ.* **1990**, *24A*, 1939.
- Chase, M. W., Jr.; Davies, C. A.; Downey, J. R., Jr.; Frurip, D. J.; McDonald, R. A.; Syverud, A. N. *J. Phys. Chem. Ref. Data* **1985**, *14* (Suppl. I).
- Nobes, R. H.; Radom, L. *Chem. Phys. Lett.* **1992**, *189*, 554.
- Curtiss, L. A.; Nobes, R. H.; Pople, J. A.; Radom, L. *J. Chem. Phys.* **1992**, *97*, 6766.
- Ruscic, B.; Berkowitz, J. *J. Chem. Phys.* **1993**, *98*, 2568.
- DeMore, W. B.; Sander, S. P.; Golden, D. M.; Hampson, R. F.; Kurylo, M. J.; Howard, C. J.; Ravishankara, A. R.; Kolb, C. E.; Molina, M. *J. Chemical Kinetics and Photochemical Data for Use in Stratospheric Modeling*; JPL Publication 92-20; Jet Propulsion Laboratory: Pasadena, CA, 1992.
- Seakins, P. W.; Pilling, M. J. *J. Phys. Chem.* **1991**, *95*, 9878.
- Wine, P. H.; Nicovich, J. M.; Stickel, R. E.; Zhao, Z.; Shackelford, C. J.; Kreutter, K. D.; Daykin, E. P.; Wang, S. In *The Tropospheric Chemistry of Ozone in the Polar Regions*; NATO ASI Series, Vol. 17; Niki, H., Becker, K. H., Eds.; Springer-Verlag: Berlin, 1993; pp 385–395.
- Stickel, R. E.; Zhao, Z.; Wine, P. H. To be published.
- McKee, M. L. Private communication.
- Sverdlov, L. M.; Kovner, M. A.; Krainov, E. P. *Vibrational Spectra of Polyatomic Molecules*; Wiley: New York, 1974.
- Durig, J. R.; Griffin, M. G. *J. Chem. Phys.* **1977**, *67*, 2220.
- Shum, L. G. S.; Benson, S. W. *Int. J. Chem. Kinet.* **1985**, *95*, 27.
- See, for example: Knox, J. H. *Molecular Thermodynamics*; Wiley-Interscience: London, 1971.
- Baker, J.; Dyke, J. M. *Chem. Phys. Lett.* **1993**, *213*, 257.
- Nourbakhsh, S.; Norwood, K.; Yin, H.-M.; Liao, C.-L.; Ng, C. Y. *J. Chem. Phys.* **1991**, *95*, 5014.
- Ma, Z.-X.; Liao, C.-L.; Yin, H.-M.; Ng, C. Y.; Chiu, S.-W.; Ma, N. L.; Li, W.-K. *Chem. Phys. Lett.* **1993**, *213*, 250.
- McCullough, J. P.; Hubbard, W. N.; Frow, F. R.; Hossenlopp, I. A.; Waddington, G. *J. Am. Chem. Soc.* **1957**, *79*, 561.
- Seakins, P. W.; Pilling, M. J.; Niiranen, J. T.; Gutman, D.; Krasnoperov, L. N. *J. Phys. Chem.* **1992**, *96*, 9847.
- Seetula, J. A.; Russell, J. J.; Gutman, D. *J. Am. Chem. Soc.* **1990**, *112*, 1347.
- Mozurkewich, M.; Benson, S. W. *J. Phys. Chem.* **1984**, *88*, 6429.
- McEwen, A. B.; Golden, D. M. *J. Mol. Struct.* **1990**, *224*, 357.
- Russell, J. J.; Seetula, J. A.; Gutman, D. *J. Am. Chem. Soc.* **1988**, *110*, 3092.
- Chen, Y.; Tschuikow-Roux, E.; Rank, A. *J. Phys. Chem.* **1991**, *95*, 9832.
- Chen, Y.; Rank, A.; Tschuikow-Roux, E. *J. Phys. Chem.* **1991**, *95*, 9900.